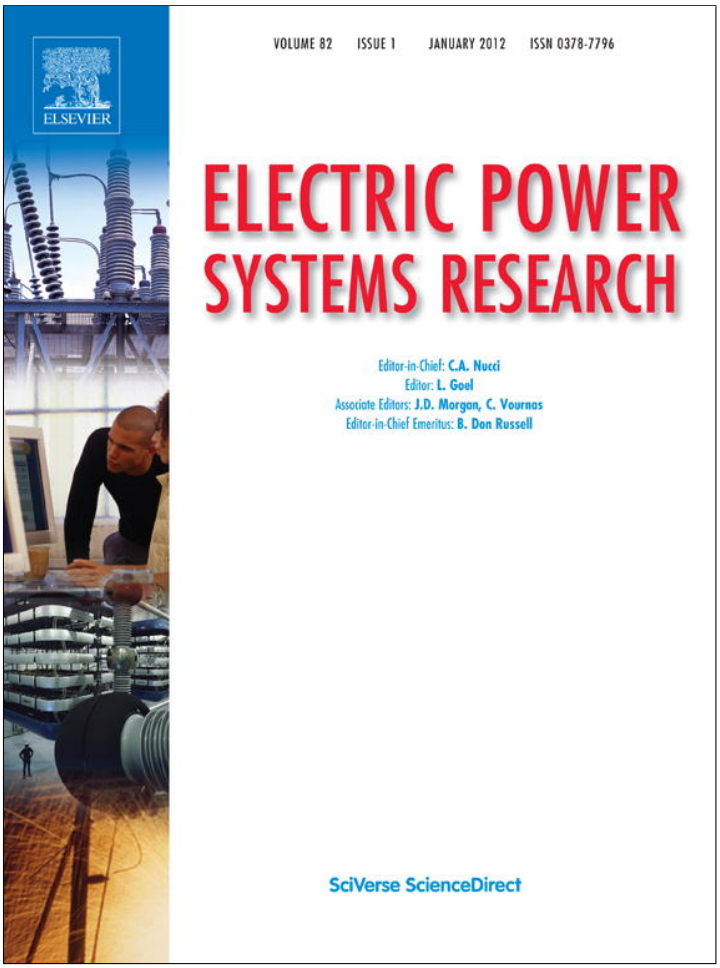

(This is a sample cover image for this issue. The actual cover is not yet available at this time.)

Electric Power Systems Research 89 (2012) 204–214

Contents lists available at SciVerse ScienceDirect

Electric Power Systems Research

journal homepage: www.elsevier.com/locate/epsr

Multi-machine power system stability improvement using an observer-based nonlinear controller

A.E. Leon [a,*], J.M. Mauricio [b], J.A. Solsona [a]

[a] Instituto de Investigaciones en Ingeniería Eléctrica (IIIE) "Alfredo Desages" (UNS-CONICET), Universidad Nacional del Sur (DIEC-UNS), Avenida Alem 1253, 8000 Bahía Blanca, Argentina

[b] Department of Electrical Engineering, University of Seville, 41092 Seville, Spain

ARTICLE INFO

Article history:
Received 8 November 2011
Received in revised form 20 January 2012
Accepted 23 January 2012

Keywords:
Decentralized excitation control
Nonlinear observer
Multi-machine power system
Nonlinear control
Power system stability

ABSTRACT

Control and operation of electric networks undergo several changes due to growing energy coming from renewable sources and demanding power quality standards. New dynamic load features also pose a challenge to grid designers. In addition, economic reasons, an increasing demand and remote generation push transmission lines to their stability limits causing oscillation modes to become more lightly damped. In this context, controllers and devices are used to enhance the performance of the new power systems. In this work, an observer-based controller to improve stability in power systems, by using the excitation of synchronous generators, is introduced. The strategy goal is to attain maximum damping injection and to increase the transient stability, while good voltage regulation performance is maintained. The proposed strategy presents two important features from the implementation point of view. First, the controller only needs sensing currents and rotor speed, and second, previous knowledge of network parameters and topology is not required. Several comparisons in multi-machine scenarios with current power system stabilizers are presented. These studies confirm the viability and the performance improvement when conventional solutions are replaced by the proposed approach.

1. Introduction

Currently, both planning and operation of power systems are changing due to several reasons. New technologies based on power electronics, such as flexible ac transmission systems (FACTS) (high-voltage direct current transmissions, static synchronous compensators, etc.) and distributed generation are being introduced [1–3]. The installed capacity on renewable energies (wind energy, photo-voltaic generation, etc.) is also increasing in a fast way [4–6]. In many power networks exist great distances between places where the energy is generated and where it is consumed. Consequently, groups of generators behave like areas and oscillations among them can produce great blackouts [7,8]. Besides, power systems operate close to stability limits due to transport and economic reasons. In this context, multi-machine power system stability arises as a very important subject to be deeply analyzed by engineers and researchers. Classical control schemes needed to be updated, and new and enhanced strategies to improve transient stability and voltage regulation in current and future power system scenarios must be found.

Control using the excitation of synchronous generators is a viable option to improve the stability margin, when economic constraints do not allow to use FACTS equipment. In this way, a cheaper solution based on the existing power facilities is obtained. The improvement of excitation controllers is also important because it is expected that future smart grids include both excitation controllers and FACTS equipments, working in a coordinated way.

One of the first studies on excitation control for stabilizing power systems is reported in [9]. There, oscillations are damped by using a power system stabilizer (PSS). This kind of controllers adds a stabilizing signal in the excitation system, and they are based on robust transfer functions to be tuned via linear techniques around an operating point. However, due to the generator behavior is nonlinear, this technique is not completely appropriate for large disturbances such as topology changes and short circuits. In such cases, PSS performance could vary causing stability problems. Taking into account this negative aspect of PSS controllers, nonlinear control techniques were introduced to improve performance in the presence of large disturbances which push the machine states out of

* Corresponding author at: Instituto de Investigaciones en Ingeniería Eléctrica (IIIE) "Alfredo Desages" (UNS-CONICET), Departamento de Ingeniería Eléctrica y de Computadoras, Universidad Nacional del Sur (UNS), Avenida Alem 1253, 8000 Bahía Blanca, Argentina. Tel.: +54 291 459 5101x3338; fax: +54 291 459 5154.
E-mail addresses: aleon@ymail.com (A.E. Leon), j.m.mauricio@ieee.org (J.M. Mauricio), jsolsona@uns.edu.ar (J.A. Solsona).

0378-7796/$ – see front matter © 2012 Elsevier B.V. All rights reserved.
doi:10.1016/j.epsr.2012.01.022

its nominal operating point. Strategies based on feedback linearization can be found in the following pioneer works [10–14], being those proposals continued in [15,16]. A design based on a Lyapunov technique, named L_gV control, was presented in [17]. Stabilization by energy-shaping was proposed in [18]. Adaptive and discrete predictive controllers were reported in [19–22]. Back-stepping and sliding mode techniques can also be found in [23–25]. All previously cited works present decentralized controllers because they only use local measurements. On the other hand, nonlinear centralized controllers have been proposed in [26–28]. In order to construct nonlinear controllers, feedback linearization is often preferred, because it presents high-performance and it allows tuning the controller through several ways. For example, in [27,29] an adaptive control based on feedback linearization was presented. In [30] feedback linearization was used and gains were set via optimal control; whereas, in [31,32] the tuning was made by using robust control techniques.

A power network is a complex system and there are many specifications to be satisfied. For these reasons, many times controllers are developed under several simplifications and/or they partially satisfy the specifications. An often used assumption considers symmetrical dq inductances (i.e. $L_q = L'_q = L'_d$), for instance, in Refs. [17,18,27,28,30,31,33]. Sometimes, only load angle control is considered without taking into account the voltage regulation [22,27,28,30]. Other works address the problem assuming an infinite bus in the system [10,14,16,17,19,29,34–36]. Some authors assume that generator internal states are available (load angle δ or transient electromotive force voltages (EMF) e'_q, e'_d) [13,15–17,27,28,34,36–40], or they build observer-based controllers measuring the load angle δ [25,34,38,39]. Nevertheless, it must be considered that load angle and dq-axis transient EMFs are not measurable in generating stations. A nonlinear observer to estimate the load angle from the generator electrical power, currents and rotor speed was proposed in [41,42]. However, the observer gains were calculated using a Taylor linearization around a particular equilibrium point, reducing the observer performance beyond the point of tuning.

In order to obtain a more precise and easily implementable control strategy, the above aspects should be reconsidered. Generators based on steam turbine could be better modeled with asymmetrical dq inductances. The requirement of good post-fault voltage regulation must also be included. Besides, regarding the implementation aspects, the availability of sensors of the variables to be fed back must be taken into account. Robustness against parameters; network topology uncertainties; and large disturbances must also be provided by the control law.

Due to the above-mentioned issues, this paper proposes a controller to improve the stability margin in a multi-machine power system via nonlinear decentralized excitation control of synchronous generators. Its design is based on the feedback linearization technique; considers asymmetrical dq inductances ($L_q \neq L'_q \neq L'_d$); and only easily measurable variables are used to construct the controller (current and rotor speed states are fed back). In order to obtain the generator internal states, needed in the control stage, a nonlinear observer is used. The nonlinear observer gains are calculated by using the Lyapunov theory. Not only the strategy increases the transient stability in multi-machine power systems, but also it provides good post-fault voltage regulation. Besides, it is robust against parameter uncertainties and large disturbances, being the network knowledge not needed.

The rest of the paper is organized as follows. Section 2 describes the model of power system components. In Section 3 the control strategy is presented. In Section 4 a static open-loop technique to obtain the generator internal states is introduced. In Section 5 the proposed nonlinear observer used to estimate the generator internal states is designed. In Section 6 the controller performance evaluation, discussions and multi-machine tests are presented. Finally conclusions are drawn in Section 7.

Table 1
State variable definitions.

Description	Symbol
Load angle of the generator i referred to the bus r	δ_{ir}
Generator rotor speed	ω
d, q axis transient EMF	e'_d, e'_q
d, q axis generator stator current	i_d, i_q
D, Q axis generator stator current	i_D, i_Q
d, q axis high-side transformer voltage	v_d, v_q
D, Q axis high-side transformer voltage	v_D, v_Q
Electromagnetic and mechanical torque	T_e, T_m
Exciter output voltage	e_{fd}

2. Multi-machine power system model

2.1. Local model of synchronous generators

The local model presents the synchronous generator with its step-up transformer connected to a generic bus "r" of the power system network. Because steam and hydraulic generators are to be included, a two-axis dynamic model, widely used in transient stability studies [16,18,26], is considered [43],

$$\dot{\delta}_{ir} = \Omega_B(\omega_i - \omega_{ri}), \tag{1}$$

$$2H_i\dot{\omega}_i = T_{mi} - T_{ei} - D_{bi}\omega_i - K_{di}(\omega_i - \omega_{ri}), \tag{2}$$

$$T'_{d0i}\dot{e}'_{qi} = -e'_{qi} + (L_{di} - L'_{di})i_{di} + e_{fdi}, \tag{3}$$

$$T'_{q0i}\dot{e}'_{di} = -e'_{di} - (L_{qi} - L'_{qi})i_{qi}, \tag{4}$$

and $T_{ei} = e'_{qi}i_{qi} + e'_{di}i_{di} + (L'_{di} - L'_{qi})i_{qi}i_{di}$, where "i"-subindex stands for the ith generator of the system. The stator algebraic constraints are,

$$0 = R_{sri}i_{di} + L'_{qri}i_{qi} - e'_{di} + v_{di}, \tag{5}$$

$$0 = R_{sri}i_{qi} - L'_{dri}i_{di} - e'_{qi} + v_{qi}, \tag{6}$$

where the following definitions apply,

$$\begin{aligned} L_{dri} &\triangleq L_{di} + L_{ri}, & L_{qri} &\triangleq L_{qi} + L_{ri}, \\ L'_{dri} &\triangleq L'_{di} + L_{ri}, & L'_{qri} &\triangleq L'_{qi} + L_{ri}, \\ R_{sri} &\triangleq R_{si} + R_{ri}. \end{aligned} \tag{7}$$

Dynamic states and model parameters are in the per unit system. They are defined in Table 1 and 2. In both tables, notation to be used in the rest of the article has also been included.

A synchronous DQ reference frame is defined by synchronizing with the high-side transformer voltage $v_{ri}e^{j\theta_{ri}}$. In this synchronous DQ reference frame, the high-side transformer voltage is expressed as $v_{ri}e^{j0^\circ} = v_{Qi} + jv_{Di}$. The high-side transformer voltage, in the local dq reference frame, is given by $v_{ri}e^{-j\delta_{ir}} = v_{qi} + jv_{di}$. Therefore,

$$v_{di} = -v_{ri}\sin\delta_{ir}, \tag{8}$$

$$v_{qi} = v_{ri}\cos\delta_{ir}. \tag{9}$$

Current $i_ie^{j(\theta_{ri}-\phi_i)}$ can also be expressed in the synchronous DQ reference frame as $i_ie^{-j\phi_i} = i_{Qi} + ji_{Di}$ and in the local dq reference frame as $i_ie^{-j(\delta_{ir}+\phi_i)} = i_{qi} + ji_{di}$. These reference frames are shown in Fig. 1. In this point must be remarked a very important implementation issue. Variables in the local dq reference frame are not available to be fed back, because they are referred to a frame which depends on the non-measurable load angle δ_{ir}. However, actual sensors can be used to measure currents and voltages when they are expressed in

Table 2
WECC system parameters and data.

Description	Parameter	Value		
		Gen#1	**Gen#2**	**Gen#3**
Synchronous generators				
Rated power	S_N (MVA)	247.50	192.00	128.00
Base angular frequency	Ω_B (r/s)	$2\pi60$	$2\pi60$	$2\pi60$
Generator inertia constant	H (s)	23.640	6.4000	3.0100
d-axis inductance	L_d	0.1460	0.8958	1.3125
d-axis transient inductance	L'_d	0.0608	0.1198	0.1813
q-axis inductance	L_q	0.0969	0.8645	1.2578
q-axis transient inductance	L'_q	0.0969	0.1969	0.2500
d-axis transient open circuit time constant	T'_{d0} (s)	8.9600	6.0000	5.8900
q-axis transient open circuit time constant	T'_{q0} (s)	0.3100	0.5350	0.6000
Amortisseur damping coefficient	K_d	9.5756	2.4881	0.9802
Mechanical losses damping coefficient	D_b	0.0000	0.0000	0.0000
Step-up transformer and stator resistances	R_r, R_s	0.0000	0.0000	0.0000
Step-up transformer inductance	L_r	0.0576	0.0625	0.0586
Excitation systems				
Amplifier stage gain	K_A	210.00	210.00	210.00
Amplifier stage time constant	T_A (s)	0.0100	0.0100	0.0100
Minimum exciter voltage limit	$E_{fd}^{\min}$	−6.000	−6.000	−6.000
Maximum exciter voltage limit	$E_{fd}^{\max}$	6.4300	6.4300	6.4300
Gen. terminal &regulator refer. voltages	v_t, v_t^*	1.0400	1.0250	1.0250
Power system stabilizer gain	K_S	–	8.2550	0.0820
Washout time constant	T_{wo} (s)	–	5.0000	5.0000
Phase compensation time constant	T_1 (s)	–	0.2010	0.6310
Phase compensation time constant	T_2 (s)	–	0.0500	0.0500
Phase compensation time constant	T_3 (s)	–	0.1370	0.6290
Phase compensation time constant	T_4 (s)	–	0.0500	0.0500
Turbine-governor				
Water time constant	T_w (s)	2.0000	–	–
Permanent droop	R_{Dp}	0.0500	0.0500	0.0500
Transient droop	R_{Dt}	0.0909	–	–
Dashpot time constant	T_{Rt} (s)	9.0000	–	–
High pressure power fraction	F_{HP}	–	0.3000	0.3000
Intermed. and low pressure power fractions	F_{IP}, F_{LP}	–	0.7000	0.7000
Steam chest time constant	T_{CH} (s)	–	0.3000	0.3000
Reheater time constant	T_{RH} (s)	–	7.0000	7.0000
Gate/valve rate limit	$\dot{G}^{\min,\max}\left(\frac{1}{s}\right)$	0.1600	0.3000	0.3000
Proposed nonlinear control and observer parameters				
Pole placement of control	μ	–	11.000	11.000
Proportional gain of voltage control	K_{Pvt}	–	0.1000	0.5000
Integral gain of voltage control	K_{Ivt}	–	0.1400	0.7000
Observer gain	g	–	200.00	200.00
Induction motors and static loads		**A**	**B**	**C**
Stator winding resistance	R_s	0.0068	0.0068	0.0068
Motor plus driven load inertia constant	$H(s)$	0.5000	0.5000	0.5000
Induction motor inductance	L_{dq}	3.5000	3.5000	3.5000
Induction motor transient inductance	L'_{dq}	0.1700	0.1700	0.1700
Transient open circuit time constant	T'_{dq0} (s)	0.5300	0.5300	0.5300
Per unit of load that is constant impedance	α_Z	0.2000	0.2000	0.2000
Per unit of load that is const current	α_I	0.4000	0.4000	0.4000
Per unit of load that is const power	α_P	0.1750	0.1750	0.1750
Per unit of load that is dynamic	α_{IM}	0.2250	0.2250	0.2250

Except where indicated, parameters are in p.u. on 100MVA base.

the synchronous DQ reference frame. Relationships between both reference frames can be obtained as,

$$v_{Di} = v_{di}\cos\delta_{ir} + v_{qi}\sin\delta_{ir}, \tag{10}$$

$$v_{Qi} = v_{qi}\cos\delta_{ir} - v_{di}\sin\delta_{ir}, \tag{11}$$

$$i_{Di} = i_{di}\cos\delta_{ir} + i_{qi}\sin\delta_{ir}, \tag{12}$$

$$i_{Qi} = i_{qi}\cos\delta_{ir} - i_{di}\sin\delta_{ir}. \tag{13}$$

2.2. Excitation system and power system stabilizer

The performance of the proposed strategy is compared with a conventional approach consisting of an automatic voltage regulator type IEEE-ST1A, and a power system stabilizer type IEEE-PSS1A (see IEEE Standard 421.5-2005 [44] for further model details).

2.3. Steam and hydraulic turbine-governor

A third-order dynamic model is used to represent the steam turbines. This model takes into account the steam chest and reheater dynamics. The governor and valve servomotor models are also

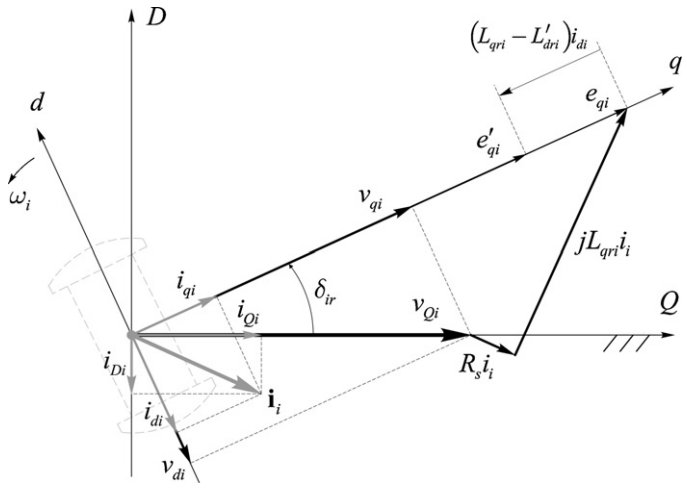

Fig. 1. Synchronous and local reference frames of each generator.

considered [45]. Hydraulic turbines are modeled by a nonlinear fourth-order model. This model is composed of a governor and includes a transient term to compensate the nonminimum-phase behavior of the hydraulic turbine [46].

2.4. Composite load model

It is known that both dynamics and stability strongly depend on the loads. In this work, the load model follows recommendations introduced in [47,48] and references therein. In those works, it is recommended to consider model of loads composed by both static and dynamic components. The static component is represented by a ZIP load, which consists in a combination of impedance, current and power constant loads. On the other hand, induction motors are considered as dynamic loads. These motors are represented by a third-order transient model. Percentages of static loads and motor parameters are indicated in Table 2.

3. Nonlinear decentralized excitation control

3.1. Input–output feedback linearization of the synchronous generator

In this section the feedback linearization control strategy is described for completeness of the work. More details about this technique, applied to the synchronous generator, can be consulted in previous works, for example in Refs. [10–16]. This strategy allows to cancel the model nonlinearities linearizing the input–output dynamics. Since the system (1)–(6) is a set of differential algebraic equations (DAE), the algebraic states i_{di} and i_{qi} are calculated from (5) and (6) and replaced in (1)–(4). In this way, a set of ordinary differential equations (ODE) representing the generator dynamics becomes,

$$\dot{\delta}_{ir} = \Omega_B(\omega_i - \omega_{ri}), \tag{14}$$

$$2H_i\dot{\omega}_i = T_{mi} - T_{ei} - D_{bi}\omega_i - K_{di}(\omega_i - \omega_{ri}), \tag{15}$$

$$T'_{d0i}\dot{e}'_{qi} = -\frac{L_{dri}e'_{qi}}{L'_{dri}} + \frac{(L_{dri}-L'_{dri})}{L'_{dri}}v_{ri}\cos\delta_{ir} + e_{fdi}, \tag{16}$$

$$T'_{q0i}\dot{e}'_{di} = -\frac{L_{qri}e'_{di}}{L'_{qri}} - \frac{(L_{qri}-L'_{qri})}{L'_{qri}}v_{ri}\sin\delta_{ir}, \tag{17}$$

where,

$$T_{ei} = \frac{e'_{qi}}{L'_{dri}}v_{ri}\sin\delta_{ir} + \frac{e'_{di}}{L'_{qri}}v_{ri}\cos\delta_{ir} + \frac{(L'_{dri}-L'_{qri})}{L'_{dri}L'_{qri}}v_{ri}^2\cos\delta_{ir}\sin\delta_{ir}. \tag{18}$$

Since in large synchronous generators stator resistance losses are small, for simplicity resistance has been neglected. A more compact description of (14)–(17) is obtained by changing the notation as follows,

$$\dot{\mathbf{x}} = \mathbf{f}(\mathbf{x}) + \mathbf{g}u, \tag{19}$$

where

$$\mathbf{f}(\mathbf{x}) \triangleq \begin{bmatrix} a_0(x_2-1) \\ -a_1px_3\sin x_1 - a_2px_4\cos x_1 - a_4x_2 - a_5(x_2-1) + a_3p^2\cos x_1\sin x_1 + T \\ -a_6x_3 + a_7p\cos x_1 \\ -a_8x_4 - a_9p\sin x_1 \end{bmatrix},$$

$$\mathbf{g} \triangleq \begin{bmatrix} 0 & 0 & 1 & 0 \end{bmatrix}^T,$$

with,

$$\mathbf{x}^T \triangleq \begin{bmatrix} x_1 & x_2 & x_3 & x_4 \end{bmatrix} = \begin{bmatrix} \delta_{ir} & \omega_i & e'_{qi} & e'_{di} \end{bmatrix},$$

$$u \triangleq \frac{e_{fdi}}{T'_{d0i}}, \quad T \triangleq \frac{T_{mi}}{2H_i}, \quad p \triangleq v_{ri}, \quad \omega_{ri} = 1,$$

$$a_0 \triangleq \Omega_B, \quad a_1 \triangleq \frac{1}{2H_iL'_{dri}}, \quad a_2 \triangleq \frac{1}{2H_iL'_{qri}}, \quad a_3 \triangleq a_1 - a_2,$$

$$a_4 \triangleq \frac{D_{bi}}{2H_i}, \quad a_5 \triangleq \frac{K_{di}}{2H_i}, \quad a_6 \triangleq \frac{L_{dri}}{T'_{d0i}L'_{dri}},$$

$$a_7 \triangleq \frac{L_{dri}-L'_{dri}}{T'_{d0i}L'_{dri}}, \quad a_8 \triangleq \frac{L_{qri}}{T'_{q0i}L'_{qri}}, \quad a_9 \triangleq \frac{L_{qri}-L'_{qri}}{T'_{q0i}L'_{qri}}.$$

In the sequel, the controller is designed by neglecting the damping terms in the mechanical equation ($a_4 = a_5 = 0$). The purpose behind this action is not cancel the natural nonlinear damping introduced by the generator, and to obtain a more compact control law. The transformation needed for the feedback linearization is given by [49],

$$\mathbf{z} = \begin{bmatrix} x_1 \\ a_0(x_2-1) \\ a_0(T - a_1px_3\sin x_1 + p\cos x_1(a_3p\sin x_1 - a_2x_4)) \\ x_4 \end{bmatrix} \tag{20}$$

with $\mathbf{z} = [\, z_1 \quad z_2 \quad z_3 \quad z_4 \,]^T$, where $z_1 = \delta_{ir}$ is the load angle, $z_2 = \dot{z}_1 = \Omega_B(\omega_i - 1)$ is the speed deviation, and $z_3 = \dot{z}_2 = \Omega_B\dot{\omega}_i = \Omega_B\alpha_i$ is the rotor acceleration. Since the z_1 relative degree is equal to three, and (19) represents a fourth-order system, then the transformation was completed by introducing $z_4 = x_4$. The control law linearizing the system (19) results (see Eq. (6.96) in [49]),

$$u = \sigma^{-1}(v - \rho), \tag{21}$$

where σ and ρ can be written in a short notation by using Lie derivatives (see [49] for further details), resulting in this case,

$$\rho \triangleq L_{\mathbf{f}}^3 z_1 = a_0p(a_1(a_6x_3 - a_7p\cos x_1)\sin x_1 + a_2\cos x_1(a_8x_4 + a_9p\sin x_1) + a_0(x_2-1)(a_2x_4\sin x_1 + a_3p\cos 2x_1 - a_1x_3\cos x_1)) \tag{22}$$

$$\sigma \triangleq L_{\mathbf{g}}L_{\mathbf{f}}^2 z_1 = -a_0a_1p\sin x_1. \tag{23}$$

The system linearized by transformation and feedback, in the transformed coordinates $\mathbf{z}$, becomes,

$$\ddot{z}_1 = v, \tag{24}$$

$$\dot{z}_4 = -a_8z_4 - a_9p\sin z_1. \tag{25}$$

Note that two subsystems were obtained. One of them $\ddot{z}_1 = v$ relates the variable to be controlled with an auxiliary control v in a linear way. The other, $\dot{z}_4 = -a_8 z_4 - a_9 p \sin z_1$, expresses the internal dynamics remaining from the partially input–output linearized system. The system is stable in the whole operating space when z_1 is properly controlled, since z_4 is stable because $a_8 > 0$ and the nonlinear term depending on z_1 is bounded (see Eq. (25)). In order to control the system given by (24) the following state-feedback law is selected,

$$v = -\mathbf{K}\left(\begin{bmatrix} z_1 \\ z_2 \\ z_3 \end{bmatrix} - \begin{bmatrix} z_1^* \\ z_2^* \\ z_3^* \end{bmatrix}\right) = -\begin{bmatrix} K_1 \\ K_2 \\ K_3 \end{bmatrix}^T \begin{bmatrix} \delta_{ir} - \delta_{ir}^* \\ \Omega_B(\omega_i - 1) \\ \Omega_B \alpha_i \end{bmatrix}, \tag{26}$$

where K_i constant gains can be designed by linear techniques including eigenvalue assignment, optimal quadratic regulation, pole placement, etc. A critically damped response, with poles coinciding with real part equal to μ, is obtained when $K_1 = 3\mu$, $K_2 = 3\mu^2$, $K_3 = \mu^3$ are set. This last criterion was chosen in our work.

3.2. Voltage regulation control

A very important specification to be satisfied by the controller is to increase the transient stability. However, it is also needed that the same controller presents a good terminal post-fault voltage regulation [50]. It must be noted that when a controller based on the transformed states (δ_{ir}, ω_i, and α_i, see (26)) is designed, the generator terminal voltage does not appear in an explicit way. Generally, network topology changes when a fault occurs; thus, in order to keep the terminal voltage value, a new load angle reference must be calculated. In order to deal with this issue (load angle reference calculation) some solutions can be found in the literature, see for instance references [33,14,29,16,12,39,36,37,51]. A detailed description of different ways to obtain the new load angle is presented in Section 4 of [52]. In our controller, the dynamic reference technique was chosen (see Section 4.5 in [52]).

Remark 1: The proposed scheme is a decentralized controller, because it only uses local measurements. In this way, communications drawbacks among generators and distant areas are avoided.

Remark 2: The proposed controller does not need neither information on network topology and network impedances nor power flow to calculate the new equilibrium point.

Remark 3: The control strategy requires the δ_{ir} load angle and dq-axis transient EMFs e'_{qi} and e'_{di} to be implemented. As it was mentioned, the load angle and transient EMFs in a generating station are generally not available. In order to obtain these states from actual available sensors an open-loop estimator can be built like it is described in Section 4. In order to reduce the parameter sensitivity of open-loop estimators a closed-loop technique could be implemented. To this end, a new proposal is introduced in Section 5 consisting to estimate the needed states via a nonlinear observer (a closed-loop estimator). For simplicity, sub-index "i" indicating the ith generator will be omitted in the sequel.

4. Open-loop static estimator

The control law (21)–(23) needs the generator internal states $[\,\delta \quad e'_q \quad e'_d\,]$. Nevertheless, in practice, these states are not measurable. For this reason, these states must be estimated from measurable quantities, such as $[\,v_D \quad v_Q \quad i_D \quad i_Q\,]$. Equations relating both internal states and measured variables are,

$$\begin{bmatrix} \hat{\delta} & \hat{e}'_q & \hat{e}'_d \end{bmatrix}^T = \begin{bmatrix} \arccos(\beta) \\ \beta(R_{sr} i_Q - L'_{dr} i_D + v_Q) + \sqrt{1-\beta^2}\left(R_{sr} i_D + L'_{dr} i_Q + v_D\right) \\ \beta(R_{sr} i_D + L'_{qr} i_Q + v_D) - \sqrt{1-\beta^2}(R_{sr} i_Q - L'_{qr} i_D + v_Q) \end{bmatrix} \tag{27}$$

with,

$$\beta \triangleq \frac{R_{sr} i_Q - L_{qr} i_D + v_Q}{\sqrt{(R_{sr} i_D + L_{qr} i_Q + v_D)^2 + (R_{sr} i_Q - L_{qr} i_D + v_Q)^2}},$$

where the symbol $\hat{()}$ is used to indicate an estimated value. The transformation (27) can be obtained from Eqs. (5) and (6) and taking into account the reference frame rotations of Eqs. (10)–(13). Also, as it is verified $T'_{q0} \ll T'_{d0}$, which is equivalent to consider the e'_d dynamics faster than the e'_q dynamics, it is possible to assume that the d-axis transient EMF (e'_d) is an algebraic state ($T'_{q0} \cong 0$). Therefore, from (17) the following algebraic equation is obtained,

$$0 = L_{qr} e'_d + (L_{qr} - L'_{qr}) v_r \sin\delta. \tag{28}$$

The whole procedure is omitted for space reasons. Strategies employing static transformations, which are similar to that presented in Eq. (27), can be found in [23,24,30,35,51].

5. Closed-loop nonlinear estimator

As mentioned, to use an open-loop static transformation is disadvantageous from robustness point of view (*i.e.* performance in the presence of uncertainties). In order to construct a more robust estimator, an observer (closed-loop estimator) will be used to estimate the states to be fed back. By calculating e'_d from (28) and replacing in (14)–(16), the following model is obtained,

$$\dot{\delta} = \Omega_B(\omega - \omega_r), \tag{29}$$

$$2H\dot{\omega} = T_m - T_e - D_b\omega - K_d(\omega - \omega_r), \tag{30}$$

$$T'_{d0}\dot{e}'_q = -\frac{L_{dr} e'_q}{L'_{dr}} + \frac{(L_{dr} - L'_{dr})}{L'_{dr}} v_r \cos\delta + e_{fd}, \tag{31}$$

where $T_e = \frac{e'_q v_r \sin\delta}{L'_{dr}} + \frac{L'_{dr} - L_{qr}}{L_{qr} L'_{dr}} v_r^2 \cos\delta \sin\delta$. Rotor speed ($\omega$) and components of stator current (i_D and i_Q) are measured. Using the relationships (12) and (13) and Eqs. (5) and (6), these measured variables can be written as functions of the internal states, yielding,

$$i_D = \frac{v_r \sin^2\delta}{L_{qr}} + \frac{(-e'_q + v_r\cos\delta)\cos\delta}{L'_{dr}}, \tag{32}$$

$$i_Q = \frac{(L_{qr} e'_q + v_r(L'_{dr} - L_{qr})\cos\delta)\sin\delta}{L'_{dr} L_{qr}}. \tag{33}$$

In a more compact notation, the system (29)–(31) and its measurable outputs (Eqs. (32), (33) and ω) become,

$$\dot{\mathbf{x}} = \mathbf{f}(\mathbf{x}) + \mathbf{g}u, \tag{34}$$

$$\mathbf{y} = \mathbf{h}(\mathbf{x}), \tag{35}$$

where,

$$\mathbf{x} \triangleq \begin{bmatrix} \delta & \omega & e'_q \end{bmatrix}^T, \mathbf{y} \triangleq \begin{bmatrix} i_D & i_Q & \omega \end{bmatrix}^T, u \triangleq e_{fd},$$

$$\mathbf{f}(\mathbf{x}) \triangleq \begin{bmatrix} \Omega_B(\omega - \omega_r) \\ \frac{1}{2H}(T_m - T_e - K_d(\omega - \omega_r)) \\ -\frac{L_{dr}e'_q}{T'_{d0}L'_{dr}} + \frac{(L_{dr} - L'_{dr})}{T'_{d0}L'_{dr}} v_r \cos\delta \end{bmatrix},$$

$$\mathbf{g} \triangleq \begin{bmatrix} 0 & 0 & \frac{1}{T'_{d0}} \end{bmatrix}^T, \mathbf{h}(\mathbf{x}) \triangleq \begin{bmatrix} i_D & i_Q & \omega \end{bmatrix}^T.$$

The following Luenberger-like structure is implemented for the proposed nonlinear observer [53] (see Eq. (A.8) in the Appendix),

$$\dot{\hat{\mathbf{x}}} = \mathbf{f}(\hat{\mathbf{x}}) + \mathbf{g}u + \boldsymbol{\vartheta}^{-1}(\hat{\mathbf{x}})\mathbf{G}(\mathbf{y} - \mathbf{h}(\hat{\mathbf{x}})). \tag{36}$$

The complete derivation of the observer equation, stability analysis, and convergence to zero of the estimation error are provided in the Appendix. Expanding (36) results,

$$\begin{bmatrix} \dot{\hat{\delta}} \\ \dot{\hat{\omega}} \\ \dot{\hat{e}}'_q \end{bmatrix} = \begin{bmatrix} \Omega_B(\hat{\omega} - \omega_r) \\ \frac{1}{2H}(T_m - \hat{T}_e - K_d(\hat{\omega} - \omega_r)) \\ -\frac{L_{dr}\hat{e}'_q}{T'_{d0}L'_{dr}} + \frac{(L_{dr} - L'_{dr})}{T'_{d0}L'_{dr}} v_r \cos\hat{\delta} + \frac{e_{fd}}{T'_{d0}} \end{bmatrix} + \boldsymbol{\vartheta}^{-1}(\hat{\mathbf{x}}) g \left(\begin{bmatrix} i_D \\ i_Q \\ \omega \end{bmatrix} - \begin{bmatrix} \hat{i}_D \\ \hat{i}_Q \\ \hat{\omega} \end{bmatrix} \right) \tag{37}$$

where

$$\boldsymbol{\vartheta}(\mathbf{x}) = \begin{bmatrix} \frac{(L_{qr}e'_q + 2v_r(L'_{dr} - L_{qr})\cos\delta)\sin\delta}{L'_{dr}L_{qr}} & 0 & -\frac{\cos\delta}{L'_{dr}} \\ \frac{L_{qr}e'_q\cos\delta + v_r(L'_{dr} - L_{qr})\cos 2\delta}{L'_{dr}L_{qr}} & 0 & \frac{\sin\delta}{L'_{dr}} \\ 0 & 1 & 0 \end{bmatrix}.$$

In Eq. (36), it is possible to distinguish two terms. One of them $\mathbf{f}(\hat{\mathbf{x}}) + \mathbf{g}u$ is named prediction term, whereas the other one $\boldsymbol{\vartheta}^{-1}(\hat{\mathbf{x}})\mathbf{G}(\mathbf{y} - \mathbf{h}(\hat{\mathbf{x}}))$ is named correction term. The last one not only allows to fix the transient of convergence for the estimation error, but also it attenuates errors appearing in the prediction term due to, either parameter uncertainties or unmodeled dynamics. For this reason, the proposed closed-loop estimator is more robust than usually used open-loop estimators. The attenuation is proportional to the **G** norm; but the maximum value of the **G** norm is bounded by measurement uncertainties (for instance, measurement noise).

Finally, by implementing (37), robust estimates for the states needed to construct the feedback linearization control law (21) are obtained. Unlike proposals that need load angle sensors, easily available measurements are used (currents and rotor speed). Thus, from a practical implementation point of view, the proposed observer is very much attractive. A general block diagram showing the implementation of the whole observer-based controller is presented in Fig. 2.

Remark 1: Unmeasurable states are replaced by their estimates when the control law (21) is built. The acceleration α (needed in Eq. (26)) is also replaced by its estimate given by the observer. This estimate is calculated from the right-hand side of (37) ($\hat{\alpha} = \dot{\hat{\omega}}$).

Remark 2: Different from what is found in most of the literature, this proposal maintain the advantages of controlling the load angle δ (allowing high angle oscillation damping), while avoiding using sensors of generator internal states.

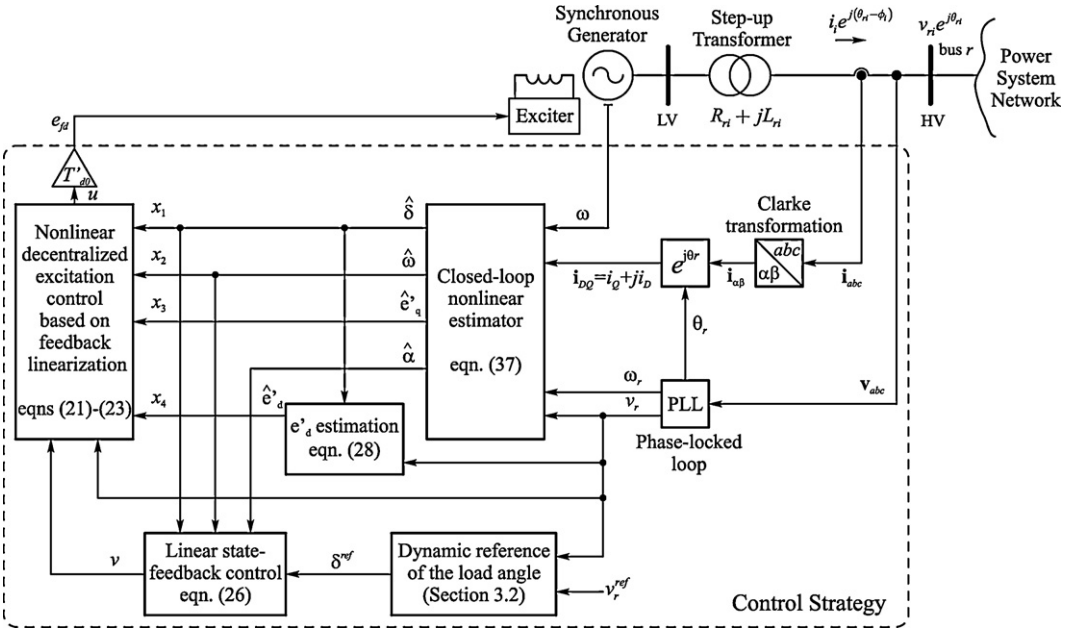

Fig. 2. Block diagram of the proposed observer-based controller.

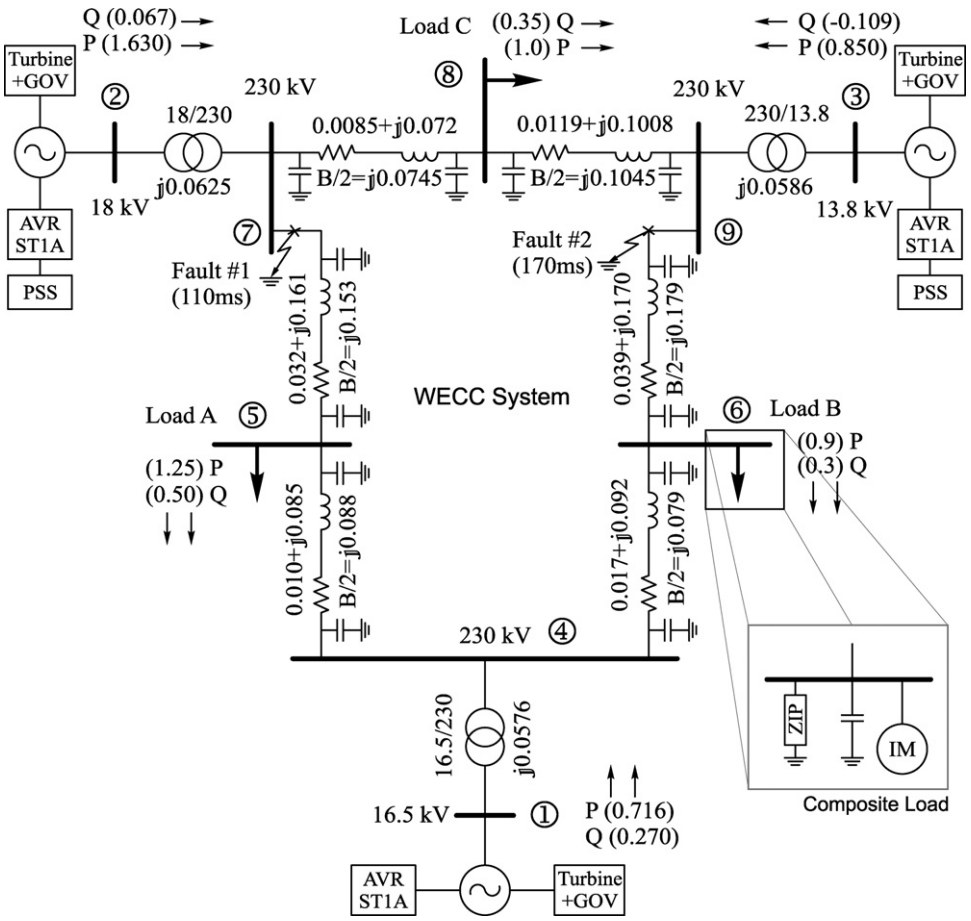

Fig. 3. WECC system power flow and line impedance diagram (parameters are in p.u. on 100MVA base).

6. Performance testing

In this Section the performance of the proposed strategy is evaluated with two systems. One of them is the Western Electricity Coordinating Council (WECC) system. This system presents oscillating modes poorly damped [54]. Much attention has been paid to this system since blackout occurred on 10 August 1996 and oscillations appeared on 4 August 2000. The other system used to show the behavior of the proposal is the IEEE 50-generator 145-bus benchmark.

6.1. WECC system test

A schematic diagram of the WECC system is shown in Fig. 3, where parameters and data used in tests were extracted from Section 2.10 of the book [55], and they were also summarized in Table 2. As mentioned, the proposed observer-based decentralized excitation control (ODEC) is compared with a conventional PSS control. To this end, the PSS controlling generators #2 and #3 are replaced by controllers based on ODEC. The PSSs parameters are equals to those given in [56], where the WECC system control was analyzed, and PSSs were tuned by using optimal control techniques.

6.1.1. Small-signal stability analysis

The eigenvalues λ_i, damping ratio ζ, and natural frequency f_n for the main oscillation modes are indicated in Table 3. Both PSS and ODEC controllers greatly improve the damping ratio in contrast to maintain the field voltage constant. From Table 3, it is worth noting that the nonlinear ODEC strategy has a better performance for small-signal disturbances than the PSS scheme (see damping ratios in bold font).

6.1.2. Large-signal stability analysis

The response to a 110ms short circuit (see fault #1 in Fig. 3) and the immediate out of service of the line 5–7 is considered. Under these circumstances, a controller performing in a good way should provide the action needed to both reach a new equilibrium point (because of the topology change) and damp the angle oscillations (because of the short circuit). The proposed controller satisfies these requirements (see Fig. 4 and 5). In Fig. 4a trajectories of the load angles of the three generators are shown. There, it can be seen that ODEC damping is bigger than PSS damping. Fig. 4b and c illustrate the system trajectories in the phase-plane. Regarding load angle and speed deviations, it can be observed that the system transient response, to reach the new equilibrium point, is better when ODEC strategy is used.

Voltage regulation of generator #2 is presented in Fig. 5a. Note that ODEC performs in a good way, attaining a fast stabilization without steady state error although the network topology has changed. Fig. 5b illustrates both PSS and ODEC control actions. The ODEC saturation time is lesser than PSS saturation time. This is an advantage of ODEC strategy, from both consumption energy and actuator stress point of view.

As mentioned in Sections 4 and 5, to estimate the generator internal states, two different open- and closed-loop techniques can be used. In Fig. 6, state trajectories of the generator #2 (solid

Table 3
Small-signal stability analysis of the WECC system.

	$\{\delta_2, \omega_2\}$ oscillatory mode			$\{\delta_3, \omega_3\}$ oscillatory mode		
	λ_i	ζ	f_n	λ_i	ζ	f_n
Constant field	$-0.238 \pm j8.36$	0.029	1.33	$-0.734 \pm j12.8$	0.057	2.03
PSS	$-3.246 \pm j7.27$	0.408	1.16	$-3.238 \pm j10.8$	0.288	1.71
ODEC	$-3.464 \pm j6.44$	**0.474**	1.03	$-16.63 \pm j9.53$	**0.868**	1.52

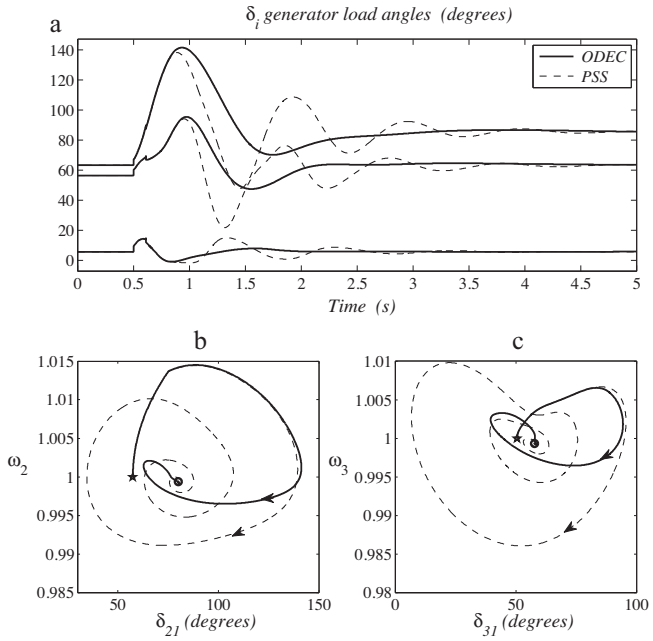

Fig. 4. Load angle evolution in the presence of the fault #1. ODEC (solid) and PSS (dashed). (a) δ_i load angle damping using PSS and ODEC schemes, (b) system trajectories in the δ–ω phase-plane of the generator #2, (c) system trajectories in the δ–ω phase-plane of the generator #3.

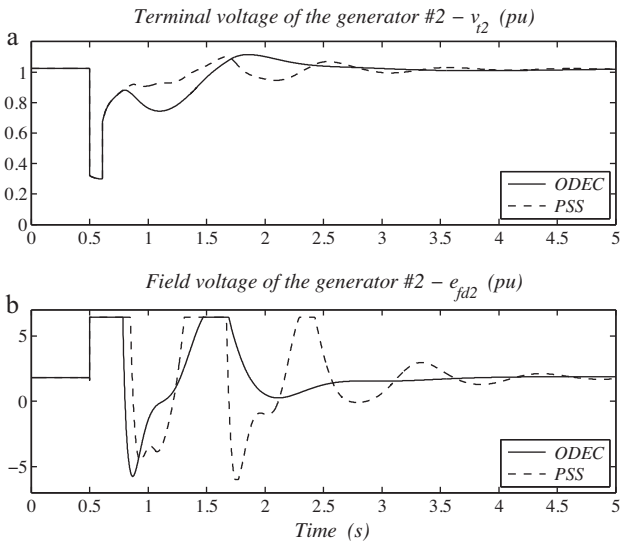

Fig. 5. (a) Terminal voltage evolution of the generator #2 in the presence of the fault #1, (b) field voltage transient responses.

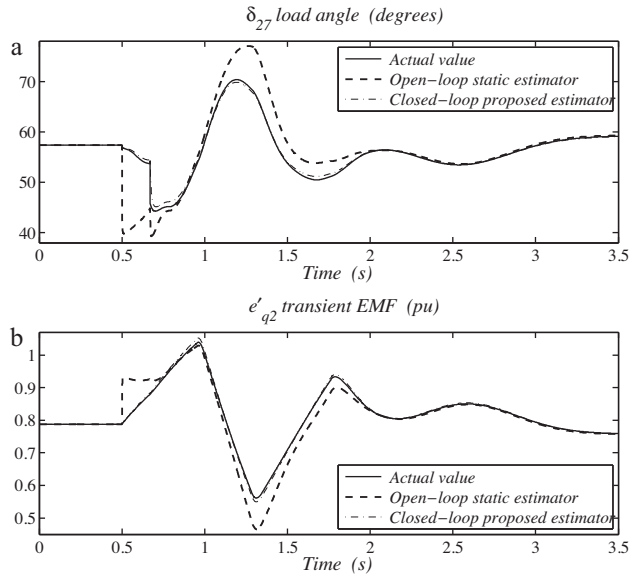

Fig. 6. Performances of the open-loop estimator and proposed closed-loop estimator. (a) Load angle estimates, (b) q-axis transient EMF estimates.

iron-rotor type) are drawn for both estimation techniques. Note that the load angle δ_{27} and transient EMF e'_{q2} estimates almost coincide with the actual values when the proposed closed-loop estimation is considered. On the other hand, the open-loop estimation presents some mismatches in the transient period.

6.2. IEEE 50-generator 145-bus system test

In this Section the IEEE 50-generator 145-bus benchmark is used to study the performance of the control strategy. Six generators are equipped with the proposed ODEC controller in order to enhance the power system stability and damp oscillations. A one-line diagram of the study area is depicted in Fig. 7.

In Fig. 8, load angle deviations are illustrated when a fault takes place in the bus 7 at $t = 1s$. Fig. 8a shows the load angle deviations when PSSs are implemented, and in Fig. 8b when the proposed schemes ODECs are installed. For simplicity, in Fig. 8c, the load angles of the first ten generators are shown, with PSS (dashed lines) and with ODEC (solid line). There, it can be seen that angle deviations, when the proposed control is used, are smaller than the case of using PSSs.

In Fig. 9a, generator frequencies are plotted for both cases PSS and ODEC. There, it can be observed that frequency deviations are smaller when the proposed strategy is used. On the other hand, field voltages of the generators, controlled by the ODEC scheme, are shown in Fig. 9b. Finally, it is noted that both angle and frequency deviations are lesser when PSSs are replaced by ODEC controllers. This allows mechanical states (δ, ω) to move away less consequently, to increase the stability margin against short circuits.

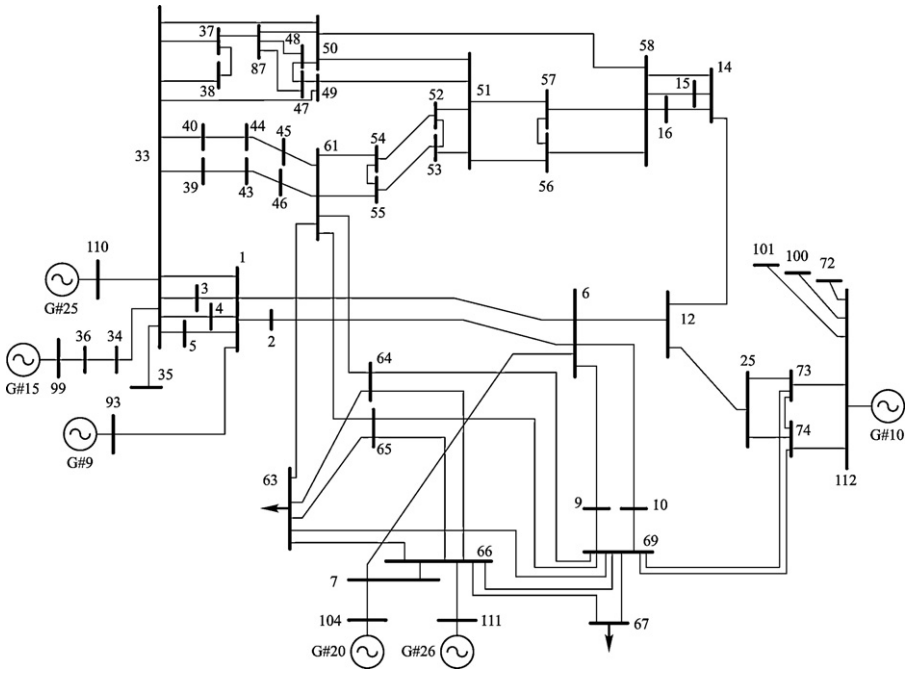

Fig. 7. IEEE 50-generator 145-bus system: a one-line diagram of the study area.

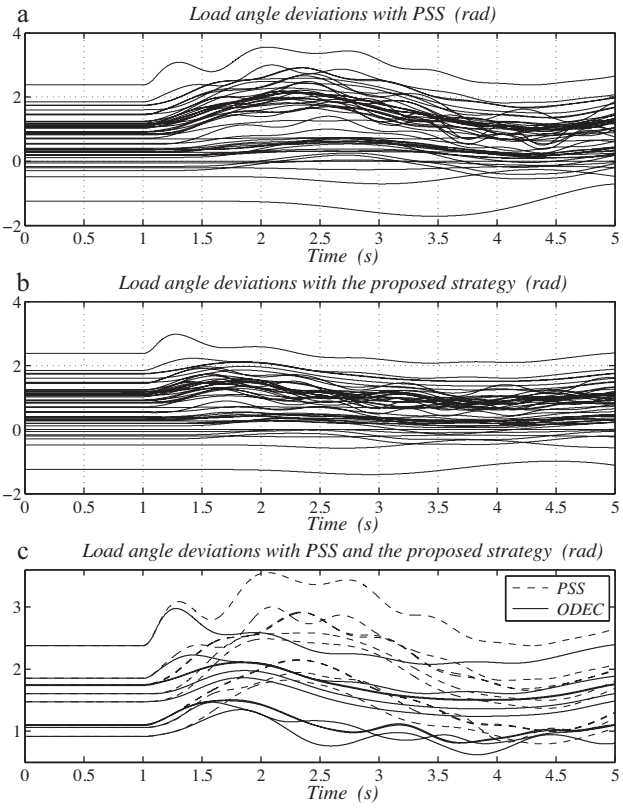

Fig. 8. Load angle deviations against a short circuit. (a) Load angle deviations with PSS, (b) load angle deviations with the proposed strategy, (c) load angle deviations with PSS and the proposed strategy (only first ten generators).

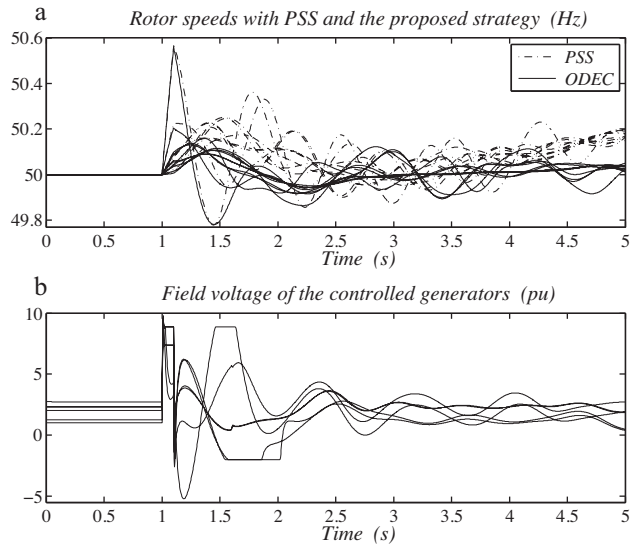

Fig. 9. (a) Generator frequencies with PSS and ODEC, (b) field voltages of the controlled generators.

7. Conclusions

An observer-based decentralized excitation control for multimachine power systems has been introduced. The main goal of the control strategy is to increase the transient stability and to obtain a good post-fault voltage regulation in spite of large disturbances and network changes.

A nonlinear observer was proposed to obtain the generator internal states from speed and current sensors. Consequently, load angle information is not needed. In addition, the controller is robust against parameter uncertainties, fault localization and network topology changes. Many tests have shown that a better transient response is obtained when PSS schemes are replaced by the proposed control law. Moreover, different to other nonlinear control approaches the strategy presents an important feature favoring

its implementation, since only easily measurable quantities are used.

Acknowledgements

This work was supported by Universidad Nacional del Sur (UNS), Consejo Nacional de Investigaciones Científicas y Técnicas (CONICET) and Agencia Nacional de Promoción Científica y Tecnológica (ANPCyT), Argentina, and by the Spanish Ministry of Education and Science (MEC) and Junta de Andalucía under grants ENE2011-24137 and P09-TEP-5170.

Appendix A.

In the following lines, the procedure to design the nonlinear observer and to guarantee the error convergence to zero is introduced. The nonlinear system given by Eqs. (34) and (35) is considered. Firstly, define $\mathbf{w}$, a smooth transformation, as follows:

$$\mathbf{w} = \mathbf{h}(\mathbf{x}) = \begin{bmatrix} i_D & i_Q & \omega \end{bmatrix}^T. \tag{A.1}$$

Then, differentiating $\mathbf{w}$ with respect to time, it results,

$$\dot{\mathbf{w}} = \frac{\partial \mathbf{h}}{\partial \mathbf{x}}\dot{\mathbf{x}} \triangleq \boldsymbol{\vartheta}(\mathbf{x})\dot{\mathbf{x}}, \tag{A.2}$$

where the matrix $\boldsymbol{\vartheta}(\mathbf{x})$ has been defined, and it represents the nonlinear observability matrix. Considering the state transformation (A.1) and (A.2), the system (34) in the $\mathbf{x}$ domain can be rewritten in the $\mathbf{w}$ domain, yielding,

$$\boldsymbol{\vartheta}^{-1}(\mathbf{x})\dot{\mathbf{w}} = \mathbf{f}(\mathbf{h}^{-1}(\mathbf{w})) + \mathbf{g}u. \tag{A.3}$$

Then, defining the following variables,

$$\tilde{\boldsymbol{\rho}}(\mathbf{w}) \triangleq \boldsymbol{\vartheta}(\mathbf{x})\mathbf{f}(\mathbf{h}^{-1}(\mathbf{w})), \tag{A.4}$$

$$\tilde{\boldsymbol{\gamma}}(\mathbf{w}) \triangleq \boldsymbol{\vartheta}(\mathbf{x})\mathbf{g}, \tag{A.5}$$

it is possible to obtain from (A.3) the below transformed system,

$$\dot{\mathbf{w}} = \tilde{\boldsymbol{\rho}}(\mathbf{w}) + \tilde{\boldsymbol{\gamma}}(\mathbf{w})u. \tag{A.6}$$

The system (A.6), in the $\mathbf{w}$ domain, presents the important characteristic that its state variables $\mathbf{w}$ are all measurable. It allows that a Luenberger-like structure will be implemented for the proposed nonlinear observer [53,57]. Therefore,

$$\dot{\hat{\mathbf{w}}} = \tilde{\boldsymbol{\rho}}(\hat{\mathbf{w}}) + \tilde{\boldsymbol{\gamma}}(\hat{\mathbf{w}})u + \mathbf{G}(\mathbf{y} - \hat{\mathbf{w}}). \tag{A.7}$$

Finally, the nonlinear observer (A.7) in the $\mathbf{w}$ domain has to be transformed back to the $\mathbf{x}$ domain applying the inverse transformation of (A.1). Consequently,

$$\dot{\hat{\mathbf{x}}} = \mathbf{f}(\hat{\mathbf{x}}) + \mathbf{g}u + \boldsymbol{\vartheta}^{-1}(\hat{\mathbf{x}})\mathbf{G}(\mathbf{y} - \mathbf{h}(\hat{\mathbf{x}})). \tag{A.8}$$

Since all estimated states have the same value, then equal gains are chosen for each state to be estimated (same convergence rate). Therefore, it is set $\mathbf{G} = g\mathbf{I}$ (with $\mathbf{I}$ the identity matrix). The nonlinear observer (A.8) was used in the estimation of the generator internal states in Section 5.

Now, the convergence to zero of the estimation error is proved. The estimation error is defined as,

$$\mathbf{e} = \mathbf{w} - \hat{\mathbf{w}}. \tag{A.9}$$

Then, the estimation-error dynamics will be given by subtracting Eq. (A.7) from (A.6), resulting,

$$\dot{\mathbf{e}} = \dot{\mathbf{w}} - \dot{\hat{\mathbf{w}}} = -g\mathbf{e} + \Delta\tilde{\boldsymbol{\rho}} + \Delta\tilde{\boldsymbol{\gamma}}u, \tag{A.10}$$

where it was defined,

$$\Delta\tilde{\boldsymbol{\rho}} \triangleq \tilde{\boldsymbol{\rho}}(\mathbf{w}) - \tilde{\boldsymbol{\rho}}(\hat{\mathbf{w}}), \tag{A.11}$$

$$\Delta\tilde{\boldsymbol{\gamma}} \triangleq \tilde{\boldsymbol{\gamma}}(\mathbf{w}) - \tilde{\boldsymbol{\gamma}}(\hat{\mathbf{w}}). \tag{A.12}$$

It is possible to find a bound to $\tilde{\boldsymbol{\rho}}$ and $\tilde{\boldsymbol{\gamma}}$ given by,

$$\|\Delta\tilde{\boldsymbol{\rho}}\| = \|\tilde{\boldsymbol{\rho}}(\mathbf{w}) - \tilde{\boldsymbol{\rho}}(\hat{\mathbf{w}})\| \le L_\rho\|\mathbf{w} - \hat{\mathbf{w}}\| = L_\rho\|\mathbf{e}\|, \tag{A.13}$$

$$\|\Delta\tilde{\boldsymbol{\gamma}}\| = \|\tilde{\boldsymbol{\gamma}}(\mathbf{w}) - \tilde{\boldsymbol{\gamma}}(\hat{\mathbf{w}})\| \le L_\gamma\|\mathbf{w} - \hat{\mathbf{w}}\| = L_\gamma\|\mathbf{e}\|, \tag{A.14}$$

where L_ρ and L_γ are $\tilde{\boldsymbol{\rho}}$ and $\tilde{\boldsymbol{\gamma}}$ Lipschitz constants, respectively. These constants can be calculated using, for example, the mean value theorem for multivariable functions or other real analysis tools. The reader interested in this subject is referred to [49,53].

In order to prove the estimation error convergence to zero, the following Lyapunov candidate function is proposed,

$$V = \mathbf{e}^T\mathbf{P}\mathbf{e}, \tag{A.15}$$

where $\mathbf{P}$ is a positive-definite matrix. Then, taking the time derivative of the function V, and after some algebraic arrangement, it is obtained,

$$\begin{aligned} \dot{V} &= \dot{\mathbf{e}}^T\mathbf{P}\mathbf{e} + \mathbf{e}^T\mathbf{P}\dot{\mathbf{e}}, \\ &= -2g\mathbf{e}^T\mathbf{P}\mathbf{e} + 2(\Delta\tilde{\boldsymbol{\rho}}^T + \Delta\tilde{\boldsymbol{\gamma}}^T u)\mathbf{P}\mathbf{e}, \end{aligned} \tag{A.16}$$

where Eq. (A.10) was used.

Since $\tilde{\boldsymbol{\rho}}$ and $\tilde{\boldsymbol{\gamma}}$ are bounded by the Lipschitz constants indicated in (A.13) and (A.14) and the input control is assumed bounded by $\|u\| \le U_{\max}$, then a bound to the time derivative of the Lyapunov function can be calculated as,

$$\begin{aligned} \dot{V} &\le -2g\lambda^{\mathbf{P}}_{\min}\|\mathbf{e}\|^2 + 2\lambda^{\mathbf{P}}_{\max}\|\mathbf{e}\|\|\Delta\tilde{\rho}^T + \Delta\tilde{\gamma}^T u\| \\ &\le -2g\lambda^{\mathbf{P}}_{\min}\|\mathbf{e}\|^2 + 2\lambda^{\mathbf{P}}_{\max}\|\mathbf{e}\|(L_\rho\|\mathbf{e}\| + L_\gamma\|\mathbf{e}\|U_{\max}) \\ &\le 2(\lambda^{\mathbf{P}}_{\max}(L_\rho + L_\gamma U_{\max}) - g\lambda^{\mathbf{P}}_{\min})\|\mathbf{e}\|^2, \end{aligned} \tag{A.17}$$

where $\lambda^{\mathbf{P}}_{\min}$ and $\lambda^{\mathbf{P}}_{\max}$ are the minimum and maximum eigenvalues of the $\mathbf{P}$ matrix, respectively. Then, from the Lyapunov stability theory, the estimation error will be asymptotically stable at the origin, if g is chosen to guarantee a negative value of the right-hand side in (A.17). As a consequence, the following inequality must be satisfied,

$$g \ge (L_\rho + L_\gamma U_{\max})\frac{\lambda^{\mathbf{P}}_{\max}}{\lambda^{\mathbf{P}}_{\min}}. \tag{A.18}$$

Note that, the proposed strategy is a nonlinear law where estimated values provided by the previously designed observer are included. In the linear case, closed-loop stability (observer-based controller plus plant) is guaranteed by using the separation theorem. Consequently, the control law and observer convergence rate can be fixed independently. As the separation theorem does not apply in the nonlinear case, when choosing the observer gains some conditions should be considered to guarantee stability. Some researches establish sufficient conditions to guarantee asymptotic convergence in the nonlinear case (see for instance [58–60]). Our observer is designed as follows: the nonlinear control strategy is calculated by assuming that the true states are available; then, observer gains are selected satisfying the conditions presented in [60]. These conditions establish how fast the observer convergence must be to guarantee closed-loop stability.

References

[1] O. Gomis-Bellmunt, J. Liang, J. Ekanayake, N. Jenkins, Voltage–current characteristics of multiterminal HVDC-VSC for offshore wind farms, Electr. Power Syst. Res. 81 (2) (2011) 440–450.

[2] A.E. Leon, J.M. Mauricio, J.A. Solsona, A. Gomez-Exposito, Software sensor-based STATCOM control under unbalanced conditions, IEEE Trans. Power Del. 24 (3) (2009) 1623–1632.

[3] A.E. Auld, J. Brouwer, G.S. Samuelsen, Analysis and visualization method for understanding the voltage effect of distributed energy resources on the electric power system, Electr. Power Syst. Res. 82 (1) (2012) 44–53.

[4] J.M. Carrasco, L.G. Franquelo, J.T. Bialasiewicz, E. Galvan, R.C.P. Guisado, M.A.M. Prats, et al., Power-electronic systems for the grid integration of renewable energy sources: a survey, IEEE Trans. Ind. Electron. 53 (4) (2006) 1002–1016.
[5] C. Zheng, M. Kezunovic, Impact of wind generation uncertainty on power system small disturbance voltage stability: a PCM-based approach, Electr. Power Syst. Res. 84 (1) (2012) 10–19.
[6] A.E. Leon, J.M. Mauricio, A. Gomez-Exposito, J.A. Solsona, An improved control strategy for hybrid wind farms, IEEE Trans. Sustainable Energy 1 (3) (2010) 131–141.
[7] G. Andersson, P. Donalek, R. Farmer, N. Hatziargyriou, I. Kamwa, P. Kundur, N. Martins, J. Paserba, P. Pourbeik, J. Sanchez-Gasca, R. Schulz, A. Stankovic, C. Taylor, V. Vittal, Causes of the 2003 major grid blackouts in North America and Europe, and recommended means to improve system dynamic performance, IEEE Trans. Power Syst. 20 (4) (2005) 1922–1928.
[8] A. Iravani, M. Karrari, O. Malik, Study of a major oscillations event in northeastern area of the Iranian power network, Electr. Power Syst. Res. 81 (7) (2011) 1292–1298.
[9] F.P. Demello, C. Concordia, Concepts of synchronous machine stability as affected by excitation control, IEEE Trans. Power Apparatus Systems 88 (4) (1969) 316–329.
[10] R. Marino, An example of a nonlinear regulator, IEEE Trans. Automatic Contr. 29 (3) (1984) 276–279.
[11] Q. Lu, Y.Z. Sun, Nonlinear stabilizing control of multimachine systems, IEEE Trans. Power Syst. 4 (1) (1989) 236–241.
[12] F.K. Mak, Design of nonlinear generator exciters using differential geometric control theories, Proc. 31st IEEE Conf. Decision Contr. 1 (1992) 1149–1153.
[13] J.W. Chapman, M.D. Ilic, C.A. King, L. Eng, H. Kaufman, Stabilizing a multimachine power system via decentralized feedback linearizing excitation control, IEEE Trans. Power Syst. 8 (3) (1993) 830–839.
[14] Y. Wang, D.J. Hill, R.H. Middleton, L. Gao, Transient stability enhancement and voltage regulation of power systems, IEEE Trans. Power Syst. 8 (2) (1993) 620–627.
[15] O. Akhrif, F.-A. Okou, L.-A. Dessaint, R. Champagne, Application of a multivariable feedback linearization scheme for rotor angle stability and voltage regulation of power systems, IEEE Trans. Power Syst. 14 (2) (1999) 620–628.
[16] Y. Guo, D.J. Hill, Y. Wang, Global transient stability and voltage regulation for power systems, IEEE Trans. Power Syst. 16 (4) (2001) 678–688.
[17] A.S. Bazanella, P.V. Kokotovic, A.S. e Silva, A dynamic extension for L_gV controllers, IEEE Trans. Automatic Contr. 44 (3) (1999) 588–592.
[18] J. Machowski, S. Robak, J.W. Bialek, J.R. Bumby, N. Abi-Samra, Decentralized stability-enhancing control of synchronous generator, IEEE Trans. Power Syst. 15 (4) (2000) 1336–1344.
[19] D. Sumina, N. Bulic, M. Miskovic, Parameter tuning of power system stabilizer using eigenvalue sensitivity, Electr. Power Syst. Res. 81 (12) (2011) 2171–2177.
[20] B. Wu, O.P. Malik, Multivariable adaptive control of synchronous machines in a multimachine power system, IEEE Trans. Power Syst. 21 (4) (2006) 1772–1781.
[21] G. Ramakrishna, O. Malik, Adaptive PSS using a simple on-line identifier and linear pole-shift controller, Electr. Power Syst. Res. 80 (4) (2010) 406–416.
[22] A.E. Leon, J.A. Solsona, J.L. Figueroa, M.I. Valla, Optimization with constraints for excitation control in synchronous generators, Energy 36 (8) (2011) 5366–5373.
[23] Q. Lu, S. Mei, W. Hu, F.F. Wu, Y. Ni, T. Shen, Nonlinear decentralized disturbance attenuation excitation control via new recursive design for multi-machine power systems, IEEE Trans. Power Syst. 16 (4) (2001) 729–736.
[24] A. Karimi, A. Al-Hinai, K. Schoder, A. Feliachi, Power system stability enhancement using backstepping controller tuned by particle swarm optimization technique, IEEE Power Eng. Soc. Gen. Meet. 2 (2005) 1388–1395.
[25] H. Huerta, A.G. Loukianov, J. Cañedo, Robust multimachine power systems control via high order sliding modes, Electr. Power Syst. Res. 81 (7) (2011) 1602–1609.
[26] F. Okou, L.-A. Dessaint, O. Akhrif, Power systems stability enhancement using a wide-area signals based hierarchical controller, IEEE Trans. Power Syst. 20 (3) (2005) 1465–1477.
[27] S. Jain, F. Khorrami, B. Fardanesh, Adaptive nonlinear excitation control of power systems with unknown interconnections, IEEE Trans. Contr. Systems Technol. 2 (4) (1994) 436–446.
[28] R. Ortega, M. Galaz, A. Astolfi, Y. Sun, T. Shen, Transient stabilization of multimachine power systems with nontrivial transfer conductances, IEEE Trans. Autom. Contr. 50 (1) (2005) 60–75.
[29] Y. Wang, D.J. Hill, R.H. Middleton, L. Gao, Transient stabilization of power systems with an adaptive control law, Automatica 30 (9) (1994) 1409–1413.
[30] Q. Lu, Y. Sun, Z. Xu, T. Mochizuki, Decentralized nonlinear optimal excitation control, IEEE Trans. Power Syst. 11 (4) (1996) 1957–1962.
[31] Y. Wang, G. Guo, D.J. Hill, Robust decentralized nonlinear controller design for multimachine power systems, Automatica 33 (9) (1997) 1725–1733.
[32] Q. Lu, S. Mei, W. Hu, Y.H. Song, M. Goto, H. Konishi, Decentralised nonlinear H_∞ excitation control based on regulation linearisation, IEE Proc. Gener. Transm. Distrib. 147 (4) (2000) 245–251.
[33] C. Zhu, R. Zhou, Y. Wang, A new decentralized nonlinear voltage controller for multimachine power systems, IEEE Trans. Power Syst. 13 (1) (1998) 211–216.
[34] J.D. Leon-Morales, K. Busawon, S. Acha-Daza, A robust observer-based controller for synchronous generators, Int. J. Electr. Power Energ. Syst. 23 (3) (2001) 195–211.
[35] G. Damm, R. Marino, F. Lamnabhi-Lagarrigue, Adaptive nonlinear output feedback for transient stabilization and voltage regulation of power generators with unknown parameters, Int. J. Robust Nonlinear Contr. 14 (9-10) (2004) 833–855.
[36] T. Lahdhiri, A.T. Alouani, Nonlinear excitation control of a synchronous generator with implicit terminal voltage regulation, Electr. Power Systems Res. 36 (2) (1996) 101–112.
[37] J. Wu, A. Yokoyama, Q. Lu, M. Goto, H. Konishi, Decentralised nonlinear equilibrium point adaptive control of generators for improving multimachine power system transient stability, IEE Proc. Gener. Transm. Distrib. 150 (6) (2003) 697–708.
[38] L. Jiang, Q.H. Wu, J.Y. Wen, Decentralized nonlinear adaptive control for multimachine power systems via high-gain perturbation observer, IEEE Trans. Circuits Syst. I: Fundamental Theory Appl. 51 (10) (2004) 2052–2059.
[39] L. Jiang, Q.H. Wu, C. Zhang, X.X. Zhou, Observer-based nonlinear control of synchronous generators with perturbation estimation, Int. J. Electr. Power Energ. Syst. 23 (5) (2001) 359–367.
[40] M.J. Jin, W. Hu, F. Liu, S.W. Mei, Q. Lu, Nonlinear co-ordinated control of excitation and governor for hydraulic power plants, IEEE Proc. Gener. Transm. Distrib. 152 (4) (2005) 544–548.
[41] W. Mielczarski, Observing the state of a synchronous generator. Part 1. Theory, Int. J. Contr. 45 (3) (1987) 987–1000.
[42] W. Mielczarski, Observing the state of a synchronous generator. Part 2. Applications, Int. J. Contr. 45 (3) (1987) 1001–1021.
[43] P. Kundur, Power System Stability and Control, McGraw-Hill, New York - USA, 1994.
[44] IEEE Standard 421. 5-2005, IEEE recommended practice for excitation system models for power system stability studies, IEEE Power Eng. Soc. (2005) 1–85.
[45] IEEE Working Group Report, Dynamic models for fossil fueled steam units in power system studies, IEEE Trans. Power Syst. 6 (2) (1991) 753–761.
[46] IEEE Working Group Report, Hydraulic turbine and turbine control models for system dynamic studies, IEEE Trans. Power Syst. 7 (1) (1992) 167–179.
[47] IEEE Task Force on Load Representation for Dynamic Performance, Standard load models for power flow and dynamic performance simulation, IEEE Trans. Power Syst. 10 (3) (1995) 1302–1313.
[48] L. Pereira, D. Kosterev, P. Mackin, D. Davies, J. Undrill, W. Zhu, An interim dynamic induction motor model for stability studies in the WSCC, IEEE Trans. Power Syst. 17 (4) (2002) 1108–1115.
[49] J.-J.E. Slotine, W. Li, Applied Nonlinear Control, Prentice-Hall, NJ, USA, 1991.
[50] A. Barakat, S. Tnani, G. Champenois, E. Mouni, A new approach for synchronous generator terminal voltage control – comparison with a standard industrial controller, Electr. Power Syst. Res. 81 (7) (2011) 1592–1601.
[51] L. Fan, A. Feliachi, Decentralized stabilization of nonlinear electric power systems using local measurements and feedback linearization, Proc. 43rd IEEE Midwest Symp. Circuits Systems 2 (2000) 638–641.
[52] A.E. Leon, J.A. Solsona, M.I. Valla, Comparison among nonlinear excitation control strategies used for damping power system oscillations, Energy Convers. Manage. 53 (1) (2012) 55–67.
[53] G. Ciccarella, M.D. Mora, A. Germani, A Luenberger-like observer for nonlinear systems, Inter. J. Contr. 57 (3) (1993) 537–556.
[54] G. Revel, A.E. Leon, D.M. Alonso, J.L. Moiola, Bifurcation analysis on a multimachine power system model, IEEE Trans. Circuits Systems I: Regular Papers 57 (4) (2010) 937–949.
[55] P.M. Anderson, A.A. Fouad, Power System Control and Stability, IEEE PRESS Power System Engineering Series, EE.UU, 1993.
[56] M.A. Abido, Optimal design of power-system stabilizers using particle swarm optimization, IEEE Trans. Energy Convers. 17 (3) (2002) 406–413.
[57] A.E. Leon, J.A. Solsona, Design of reduced-order nonlinear observers for energy conversion applications, IET Contr. Theory Applications 4 (5) (2010) 724–734.
[58] F. Esfandiari, H.K. Khalil, Output feedback stabilization of fully linearizable systems, Int. J. Contr. 56 (1992) 1007–1037.
[59] A. Teel, L. Praly, Tools for semi-global stabilization by partial state output feedback, SIAM J. Contr. Optimizat. 22 (1995) 1443–1488.
[60] M. Etchechoury, J. Solsona, C. Muravchik, Feedback linearization via state transformation using estimated states, Int. J. Syst. Sci. 32 (1) (2001) 1–7.